Condition Assessment of Highly-loaded Low-speed Bearings Using Acoustic Emission Monitoring

A Feasibility Study

Scheeren, B.; Pahlavan, Lotfollah; Kaminski, M.L.

Publication date
2018

Document Version
Accepted author manuscript

Published in
Progress in Acoustic Emission XIX

Citation (APA)
Scheeren, B., Pahlavan, L., & Kaminski, M. L. (2018). Condition Assessment of Highly-loaded Low-speed Bearings Using Acoustic Emission Monitoring: A Feasibility Study. In T. Shiotani, Y. Mizutani, & H. Yuki (Eds.), *Progress in Acoustic Emission XIX: Proceedings of the 24th International Acoustic Emission Symposium (IAES-24)* (Vol. 19, pp. 239-244). Japanese Society for Non-Destructive Inspection.

Important note
To cite this publication, please use the final published version (if applicable).
Please check the document version above.

Condition Assessment of Highly-loaded Low-speed Bearings Using Acoustic Emission Monitoring: A Feasibility Study

Bart Scheeren[1,2)], Lotfollah Pahlavan[1)], Mirek Kaminski[1)]
1) Faculty of Mechanical, Maritime and Materials Engineering, Delft University of Technology, Mekelweg 2, 2628 CD, Delft, Zuid Holland, The Netherlands.
2) Corresponding author, B.Scheeren@tudelft.nl

ABSTRACT: In the present study, feasibility of implementing an acoustic emission (AE) system for condition monitoring of highly-loaded and low-speed roller bearings has been quantitatively investigated. To evaluate the transmission of damage-induced AE signals inside the bearing and their detectability on the accessible surfaces, stress wave propagation through the complex geometry and interfaces of a representative offshore bearing has been studied experimentally. The results suggest that in the investigated frequency ranges, the AE signals that pass through the bearing rollers and their interface with the inner and outer raceways can potentially remain of sufficient strength to be detected for condition assessment of these bearings.

1 INTRODUCTION

In offshore heavy-lifting, safety and reliability of systems and procedures are of extraordinary importance. Among various components of such systems, assurance of the integrity of the sheave bearings is of special concern to the operators. Operation, or the lack thereof, under harsh offshore conditions can typically result in failing seals leading to water ingestion and corrosion, or lubrication starvation leading to abrasion and cracking. With their low rotational speeds under high loads, complex geometry, and large number of moving components, to date robust non-intrusive/non-destructive assessment of the sheave bearings has remained an unresolved challenge.

On applying the concept of measuring AE for condition monitoring of bearings, Balderston [1] successfully demonstrated the potential for detection of defects prior to failure. Subsequently, several studies compared the applicability of the AE methods to vibration monitoring [2-5], demonstrating advantages for the former in high-noise environments and in low-speed applications. More recent publications have highlighted the potentials of AE for improved robustness in damage detection [6, 7] and for defect severity estimation [8, 9].

In tribology, low-speed bearings are typically considered to be those operating below 600 rpm [10]. This is a rather wide range that envelopes both extremely-slow applications such as nacelle yaw bearings in wind turbines or turret bearings in floating production, storage, and offloading (FPSO) units, and moderately-slow applications such as some marine diesel engines. Studies on slow-speed bearings are limited. For the moderately-slow applications, a study by Zhang and Friswell [11] has shown that the rotational speed may greatly influence the quality of the AE parameters. For the extremely-slow applications, a study by Miettinen and Pataniitty [12] has shown that the detectability of AE signals decreases at lower rotational speeds. In addition, in other studies with similar extremely-low rotational speeds, classification by autoregressive coefficients has shown to be successful for separating noise from damage-induced signals of both natural [13] and artificial [14] origin. The considered case of sheave bearings in offshore heavy-lifting applications, that typically range from 10 rpm to 60 rpm, seems to have not been studied sufficiently.

A number of challenges are to be overcome to improve the reliability and robustness of the condition monitoring system in heavy-lifting applications. Most prominently, sheave bearings are of a different level of scale in comparison to most bearings considered in the literature. With diameters in the order of a metre, a different wave propagation behaviour, e.g. in dispersion and attenuation, is expected that can adversely affect the detectability of the AE signals.

In this paper, the feasibility of implementing an AE system for condition monitoring of sheave bearings has been investigated. The study focusses on measurement of the transmission of AE signals through the internal components and interfaces of a bearing, i.e. from one raceway through the rollers into the other raceway. A number of different sensors have been employed to investigate the behaviour over a sufficiently-wide frequency spectrum, ranging from 30 kHz through 1000 kHz. The presented characterization of the transfer path of the AE signals can shed light on the necessary requirements for condition monitoring of sheave bearings in offshore heavy-lifting cranes.

2 METHODOLOGY

Evolution of degradation, e.g. corrosion in the rollers or crack growth in the inner raceway, inside a roller bearing is associated with release of AE signals, as schematically shown in Figure 1. Through the interfaces between the rollers and the raceways, and also partly through the lubricant, these waves propagate inside the bearings, get reflected, scattered and diffracted, and ultimately, if they turn out to be still of sufficient energy, can be detected and measured on the external surfaces of the raceways. In order to evaluate the detectability of such waves, Hsu-Nielsen sources, i.e. standard pencil lead breaks according to ASTM-E976, and receivers with different frequency

responses in the range of 30 kHz to 1000 kHz have been employed. Given the practical limitations of simulating the AE sources at the internal locations prone to degradation in practice, the simulated AE sources have been generated on the external surfaces of the bearing. Naturally, from the transfer paths investigated in such experiments, the individual transfer functions of the internal components and contact surfaces cannot directly be extracted, however, and if desired, an analytical framework can be developed at a later stage for this purpose. The differences between the transfer paths resulting from damage-induced AE and the simulated ones are schematically displayed in Figure 1 (left). Here the expected damaged-induced source is shown internally on the inner raceway. Alternatively, the artificial sources assessed experimentally are shown on the external faces of both raceways.

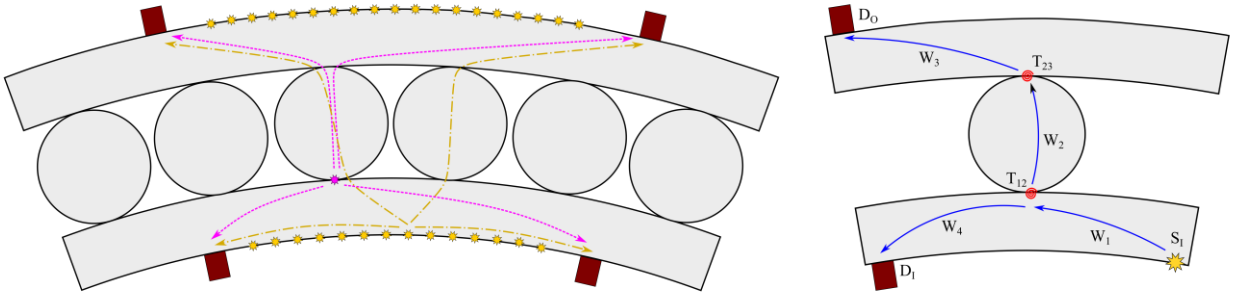

Figure 1: Representations of the experimental set-up (left) and the primary wave propagation paths (right).

Figure 1 (right) illustrates the primary wave propagation paths representative for the performed experiment. These paths may be expressed by a series of transmissions that the signal experiences before it reaches a sensor. Additionally, the signals are subject to scattering, diffraction, and mode conversion at the interfaces, which are considered to be of negligible influence on the first arriving part of the signals. For a source excited on the inner raceway described by S_I and a sensor on the same raceway with transfer function D_I, the recorded signal P_{II} can be described in the frequency domain as:

$$P_{II} = D_I W_4 W_1 S_I + P_{EII} \tag{1}$$

where W_1 and W_4 are the wave propagation (transfer) functions through finite lengths of the inner raceway (see Figure 1), and P_{EII} is a term accounting for all the neglected components of the waves and the background noise.

Alternatively, the recorded signal P_{OI} for the same source signal travelling through the roller to a sensor on the outer raceway (with transfer function D_O) can be described as:

$$P_{OI} = D_O W_3 T_{23} W_2 T_{12} W_1 S_I + P_{EOI} \tag{2}$$

where W_1, W_2 and W_3 are wave propagation functions through the inner raceway, roller, and outer raceway, respectively (see Figure 1). Also T_{12} and T_{23} denote the transmission functions of the roller-inner raceway and roller-outer raceway interfaces, respectively. P_{EOI} is a term accounting for all the neglected components of the waves and the background noise.

Under the assumption that $P_{EII} = P_{EOI} = 0$, and that the wave propagation function in both raceways is similar and non-dispersive ($W_3 = W_4$), the relative amplitude of the two signals described in Equation 1 and Equation 2 may be approximated by:

$$\frac{P_{OI}}{P_{II}} = \frac{D_O}{D_I} W_2 T_{12} T_{23} \tag{3}$$

In case the sensors have similar transfer functions and coupling, or the coupling variation is accounted for in pre-processing, D_O and D_I cancel out and the resulting quantity becomes a measure of the attenuation of the waves propagating through roller and its interfaces with the raceways.

2.1 *Experimental Set-up*

A representative offshore bearing has been instrumented on the exterior of the inner and outer raceways with standard piezoelectric acoustic emission sensors. Pencil lead breaks have been performed in various locations on both raceways to simulate AE sources. Transmission of the induced stress waves through the bearing components

has been evaluated in the frequency range of 30 kHz to 1000 kHz. Figure 2 shows several pictures of the experimental set-up.

Figure 2: The experimental set-up: a top view of the instrumented bearing (middle), R3I-AST and R6I-AST type sensors (left), and WDI-AST, VS600-Z2 and R15I-AST type sensors (right).

The investigated bearing was a cylindrical roller bearing manufactured by MTK Bearings of type F-566437.NNT. This specific bearing had been in service in a 4,000 mT heavy-lifting crane on a deep-water construction vessel. During the test the bearing was placed in a position with the circumference of the raceways in a horizontal plane. No external load was applied to the bearing.

To cover the relatively wide frequency range of interest, five sensor types were used, i.e. (i) 30 kHz resonant R3I-AST, (ii) 60 kHz resonant R6I-AST, (iii) 150 kHz resonant R15I-AST, (iv) wideband WDI-AST, and (v) 600 kHz resonant VS600-Z2. The first four sensor types are supplied by Physical Acoustics Corporation and have an integrated pre-amplifier with a gain of 40 dB. The fifth type is supplied by Vallen Systeme, and has an external AEP5H pre-amplifier with a gain of 40 dB. The transfer functions of the five sensor types are given in Figure 3. For data acquisition, an AMSY-6 system, outfitted with ASIP-2A signal processing cards, supplied by Vallen Systeme, was used. The input from the sensors were sampled at 40 MHz for both AE features and waveforms. No additional digital filtering was applied. Data was stored whenever a 40 dB threshold was crossed, whilst taking a 200 µs pre-trigger recording into account.

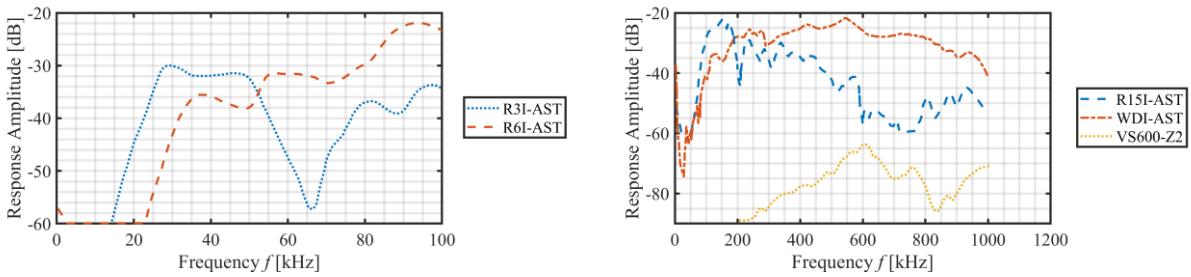

Figure 3: Typical transfer functions of the selected piezoelectric sensors. Left graph showing low-frequency sensors [15, 16], right graph showing medium and high-frequency sensors [17-19].

Simulated AE sources were generated in 45 regularly-spaced locations on the exterior of both the inner and the outer raceways over a circumferential span of about 30 degrees, as schematically shown by the stars in Figure 1. This span has been selected to guarantee the inclusion of at least two rollers in the grid of sources. For these sources, 0.5 mm 2H pencil leads were broken in accordance with the standardized Hsu-Nielsen procedure. Each location was excited with a minimum of 10 sources. On both the inner and the outer raceways, the source locations were equidistantly spaced with an increment of 5 mm. As such, the outer raceway contained 26 source locations and the inner raceway contained 19 source locations.

3 RESULTS

For every source excitation, the waveforms were recorded on both the emitted and transmitted raceways using all the five sensor types introduced before (hence five pairs of sensors). The peak amplitudes of the signals recorded in each sensor pair were obtained in the time domain. Subsequently, a comparative analysis was carried out between the different sensor types on the differences between these amplitudes for all the investigated sources.

An example of an arbitrarily-selected dataset for a source location at the leftmost end of the outer raceway (Figure 2 for reference) is shown in Figure 4, along with the frequency-domain representation of the signals at all channels. Note that to account for the possible difference in the transducers coupling functions (embedded in D_O/D_I

in Equation 3), a correction procedure was applied to the signals amplitudes. The procedure comprised a statistically-large number of Hsu-Nielsen sources at a fixed distances from each sensor, where the deviation of the mean logarithmic amplitude on the inner raceway from the expected reference signal amplitude on the outer raceway determined the correction gain (note that only the ratio D_O/D_I is of interest).

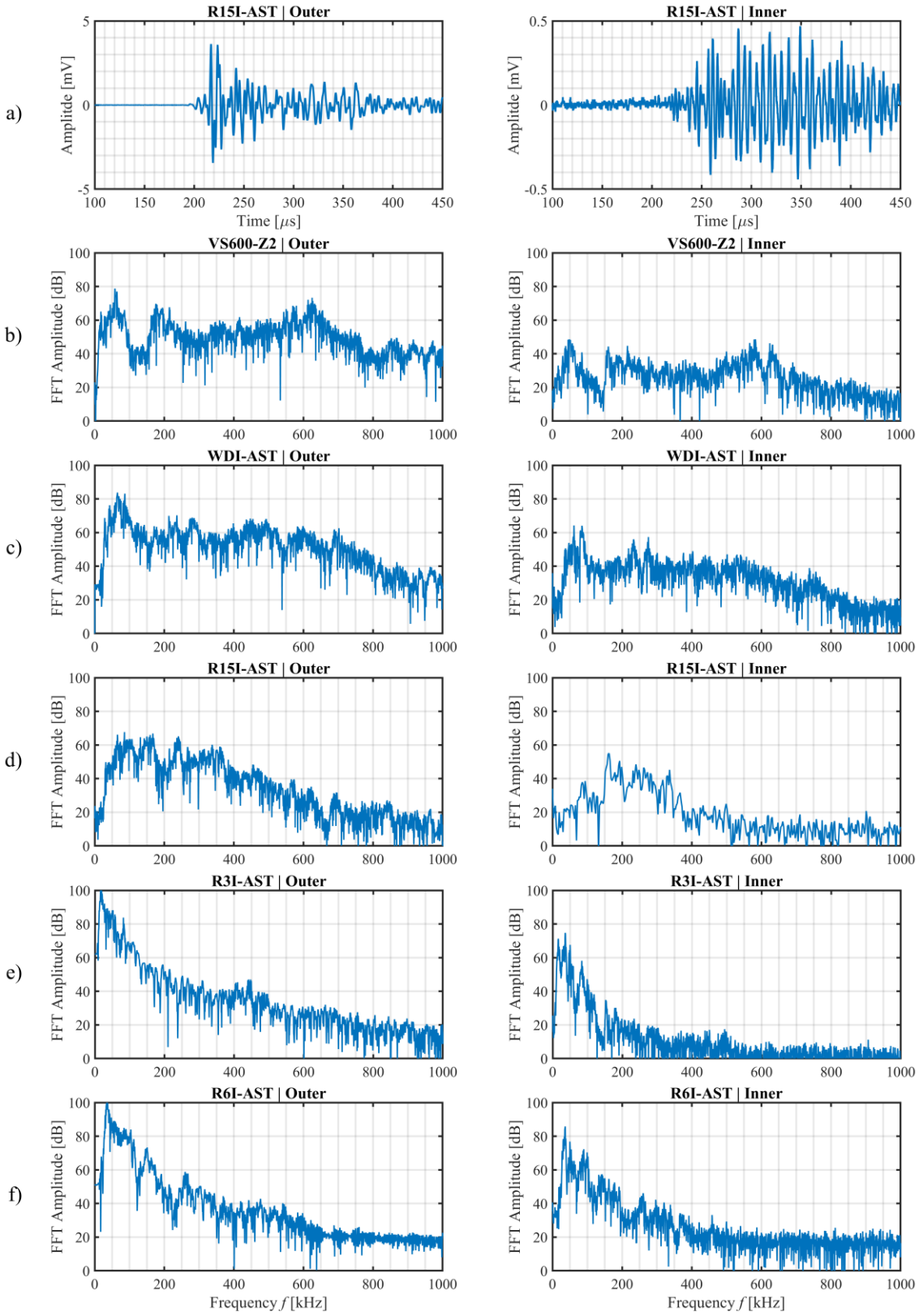

Figure 4: An example event captured by all the channels with the source on the outer raceway: time traces recorded by the R15I sensors on the outer (a, left) and inner (a, right) raceways, and frequency representation of the recorded signals on the outer (b-f, left) and inner (b-f, right) raceways.

For the sensor type WDI-AST, the peak amplitudes were recorded in four different configurations: (i) the source and the receiver both on the outer raceway, (ii) the source and the receiver both on the inner raceway, (iii) the source on the outer raceway while the receiver on the inner raceway, and (iv) the source on the inner raceway while the receiver on the outer raceway, as shown in Figure 5 (top). The signals obtained in these configurations are denoted by P_{OO}, P_{II}, P_{IO}, and P_{OI}, respectively. Source positions with greater indices have smaller circumferential distance to the respective receivers. The results suggest that the amplitude of the excited waves drop about 20 dB when passing from one raceway to the other through the rollers. The relative amplitudes, as specified by Equation 3, are shown in Figure 5 (bottom).

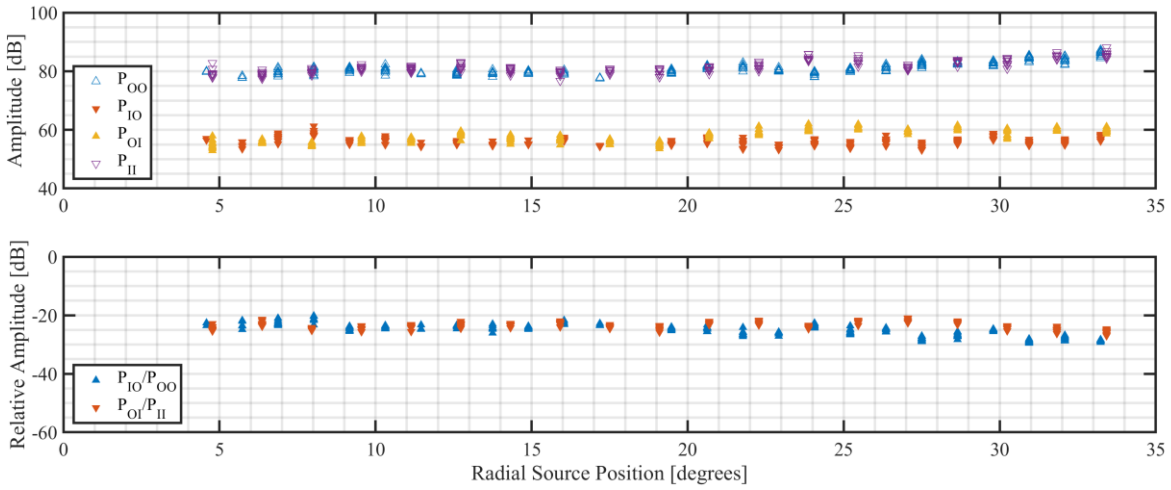

Figure 5: Amplitude of the signals recorded with the WDI-AST sensors as a function of source location: the absolute values (top), and the relative values (bottom).

Following the same procedure given above, the amplitude drop (the relative values in Figure 5) for all the five sensor types are shown in Figure 6. Both transmission paths, i.e. with the source positioned on the outer raceway and on the inner raceway, have been evaluated (therefore in total 10 sets). The mean, maximum, and minimum values have been calculated over the full range of source positions. The difference between the obtained relative values across different sensor types and propagation paths is relatively small, i.e. the variation in the mean values is in the order of ±5 dB. Although regarded small, this range was suggested by Equation 3 to be identical for all the sensors. Possible reasons for this discrepancy can originate from (i) the simplifying assumptions on insignificance of mode conversions and scatterings inside the bearing, (ii) the assumed non-negligible difference between the wave propagation functions in outer and inner raceways, (iii) the variations in the transfer functions of the sensors of the same type, and (iv) the assumption of frequency-independence in the employed coupling variation correction procedure. These issues are to be investigated in the future research.

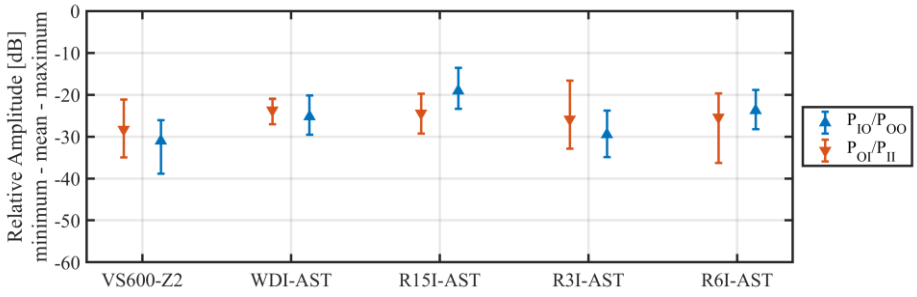

Figure 6: Overview of differential amplitude for different sensor types and transmission paths.

Considering the more likely scenarios in practice with AE sources induced by damage at or near the roller raceway interface (Figure 1), the results presented in this paper are expected to provide a conservative estimate of the amplitude drop in the AE signals. Improved reliability and accuracy for the AE system is expected for such situations.

4 CONCLUSIONS

Experiments have been performed on a bearing to study the transmission of AE signals as stress waves through its internal components and interfaces. Hsu-Nielsen sources have been excited on several locations on both the raceways. Five types of piezoelectric AE sensors covering a frequency range from 30 kHz to 1000 kHz have been applied to record the excited waves on the inner and outer raceways of the bearing. Quantitative analysis of the recorded signals suggests that (i) the transmission of AE signals through the rollers and their interfaces is potentially of sufficient strength to be recorded and distinguished from the background noise, and (ii) the amplitude drop of AE signals in transmission from one raceway to the other is in the range 20-30 dB for all the employed sensor types.

ACKNOWLEDGEMENTS

This research has been conducted within the framework of HiTeAM Joint Industry Program. Huisman Equipment is additionally acknowledged for providing the test bearings. The authors are also grateful to Eric Romeijn from Huisman Equipment and Radboud van Dijk from Heerema Marine Contractors for their extensive and constructive support.

REFERENCES

[1] Balderston, H. L., (1969). "The Detection of Incipient Failure in Bearings," *Materials Evaluation,* vol. 27, pp. 121-128.

[2] Rogers, L. M., (1979). "The application of vibration signature analysis and acoustic emission source location to on-line condition monitoring of anti-friction bearings," *Tribology International,* vol. 12, no. 2, pp. 51-58.

[3] Smith, J. D., (1982). "Vibration monitoring of bearings at low speeds," *Tribology International,* vol. 15, no. 3, pp. 139-144.

[4] McFadden, P. D. and Smith, J. D., (1984). "Acoustic Emission Transducers for the Vibration Monitoring of Bearings at Low Speeds," *Proceedings of the Institution of Mechanical Engineers, Part C: Journal of Mechanical Engineering Science,* vol. 198, no. 2, pp. 127-130.

[5] Hawman, M. W. and Galinaitis, W. S., (1988). "Acoustic emission monitoring of rolling element bearings," in *IEEE 1988 Ultrasonics Symposium Proceedings*, vol. 2, pp. 885-889.

[6] Ruiz-Cárcel, C., Hernani-Ros, E., Cao, Y., and Mba, D., (2014). "Use of Spectral Kurtosis for Improving Signal to Noise Ratio of Acoustic Emission Signal from Defective Bearings," *Journal of Failure Analysis and Prevention,* vol. 14, no. 3, pp. 363-371.

[7] Kilundu, B., Chiementin, X., Duez, J., and Mba, D., (2011). "Cyclostationarity of Acoustic Emissions (AE) for monitoring bearing defects," *Mechanical Systems and Signal Processing,* vol. 25, no. 6, pp. 2061-2072.

[8] Mba, D., (2008). "The Use of Acoustic Emission for Estimation of Bearing Defect Size," *Journal of Failure Analysis and Prevention,* vol. 8, no. 2, pp. 188-192.

[9] Al-Dossary, S., Hamzah, R. I. R., and Mba, D., (2009). "Observations of changes in acoustic emission waveform for varying seeded defect sizes in a rolling element bearing," *Applied Acoustics,* vol. 70, no. 1, pp. 58-81.

[10] Mba, D., Bannister, R. H., and Findlay, G. E., (1999). "Condition monitoring of low-speed rotating machinery using stress waves Part 1," *Proceedings of the Institution of Mechanical Engineers, Part E: Journal of Process Mechanical Engineering,* vol. 213, no. 3, pp. 153-170.

[11] He, Y., Zhang, X., and Friswell, M. I., (2009). "Defect Diagnosis for Rolling Element Bearings Using Acoustic Emission," *Journal of Vibration and Acoustics,* vol. 131, no. 6, pp. 061012-061012-10.

[12] Miettinen, J. and Pataniitty, P., (1999). "Acoustic Emission in Monitoring Extremely Slowly Rotating Rolling Bearing," in *Proceedings of the 12th International Conference on Condition Monitoring and Diagnostic Engineering Management - COMADEM '99*, Sunderland, UK, pp. 289-297: Coxmoore Publishing Company.

[13] Mba, D., Bannister, R. H., and Findlay, G. E., (1999). "Condition monitoring of low-speed rotating machinery using stress waves Part 2," *Proceedings of the Institution of Mechanical Engineers, Part E: Journal of Process Mechanical Engineering,* vol. 213, no. 3, pp. 171-185.

[14] Jamaludin, N., Mba, D., and Bannister, R. H., (2001). "Condition monitoring of slow-speed rolling element bearings using stress waves," *Proceedings of the Institution of Mechanical Engineers, Part E: Journal of Process Mechanical Engineering,* vol. 215, no. 4, pp. 245-271.

[15] MISTRAS Group, (2011: 06-06-2018). *R3I-AST Sensor*.

[16] MISTRAS Group, (2011: 06-06-2018). *R6I-AST Sensor*.

[17] MISTRAS Group, (2015: 06-06-2018). *R15I-AST Sensor*.

[18] MISTRAS Group, (2011: 06-06-2018). *WDI-AST Sensor*.

[19] Vallen Systeme, (2017: 27-06-2018). *AE-Sensor Data Sheet: VS600-Z2*.